Nanoscale

PAPER

View Article Online
View Journal | View Issue

Cite this: *Nanoscale*, 2014, **6**, 14549

Highly reproducible planar Sb_2S_3-sensitized solar cells based on atomic layer deposition†

Dae-Hwan Kim,‡[a] Sang-Ju Lee,‡[a] Mi Sun Park,[a] Jin-Kyu Kang,[a] Jin Hyuck Heo,[b] Sang Hyuk Im*[b] and Shi-Joon Sung*[a]

Received 22nd July 2014,
Accepted 8th October 2014

DOI: 10.1039/c4nr04148h

www.rsc.org/nanoscale

A high-quality Sb_2S_3 thin-absorber with controllable thickness was reproducibly formed by atomic layer deposition (ALD) technique. Compared with conventional chemical bath deposition (CBD), the Sb_2S_3 absorber deposited by ALD did not contain oxide or oxygen impurities and showed a very uniform thickness of Sb_2S_3 absorbers formed on a rough surface of dense blocking TiO_2/F-doped SnO_2 (bl-TiO_2/FTO) substrate. The planar ALD-Sb_2S_3 solar cells comprised of Au/Poly-3-hexylthiophene/ALD-Sb_2S_3/bl-TiO_2/FTO showed significantly improved power conversion efficiency of 5.77% at 1 sun condition and narrow efficiency deviation, whereas the planar CBD-Sb_2S_3 solar cells exhibited 2.17% power conversion efficiency. The high efficiency and good reproducibility of ALD-Sb_2S_3 solar cell devices is attributed to reduced backward recombination because of the inhibition of oxide defects within ALD-Sb_2S_3 absorber and the conformal deposition of very uniform Sb_2S_3 absorbers on the blocking TiO_2 surface by ALD process.

Introduction

The second generation solar cells such as organic, thin-film, and dye-sensitized solar cells (D-SSCs) have been intensively studied to satisfy the criteria of high efficiency and low cost. Among them, the D-SSCs have been considered as a promising candidate for replacing conventional silicon solar cells owing to a unique device architecture comprised of an electron conductor, sensitizer, and hole conductor. The electrons (holes) generated in the sensitizer by light illumination are immediately transported to the electron (hole) conductor, and consequently less recombination is expected. Therefore, the sensitized solar cells (SSCs) have attracted significant attention since Grätzel *et al.*[1] reported on liquid type D-SSCs and the power conversion efficiency of D-SSCs of up to ~13% at 100 mW cm^{-2} AM 1.5 G.[2]

Recently, inorganic semiconductors and quantum dots (QDs) have been of great interest because they can replace the conventional Ru/organic dyes owing to their unique properties, such as strong absorptivity, large dielectric constant, multiple exciton generation, and good stability.[3,4] Hence, many metal chalcogenides, including CdS(e),[5–8] PbS(e),[9–11] and $Sb_2S(e)_3$,[12–18] have been used as new sensitizers and their device efficiencies have been stiffly increased to over 7% at 1 sun condition.[19] Among them, the Sb_2S_3 exhibited peculiar characteristics. It forms an amorphous phase on the TiO_2 electrode at the initial processing stage, and then it is converted to crystalline stibnite by subsequent heat treatment. This may lead to the formation of an intimate junction at the TiO_2–Sb_2S_3 interface, and thus enabling the Sb_2S_3-SSCs to hold high device efficiencies.

To date, the Sb_2S_3 has been synthesized by aqueous based chemical bath deposition (CBD) method[20] to form a conformal thin-film on the TiO_2 electrode. However, the formation of antimony oxides cannot be avoided by the conventional aqueous phase CBD technique and further improvement of device performance appears to be retarded because the antimony oxides make deep traps in the gap state and cause the backward recombination of generated charge carriers.[21] Recently, Maiti *et al.*[22] reported the non-aqueous phase CBD technique for the formation of Sb_2S_3 using a single source precursor, which showed significant depression in the formation of antimony oxides. Very recently, Choi *et al.*[19] demonstrated that the antimony oxides formed by conventional CBD method can be recovered as Sb_2S_3 by post organic sulfur treatment. It is prerequisite to form pure Sb_2S_3 through certain deposition processes in order to develop efficient Sb_2S_3-SSCs.

It is also equally important to develop highly reproducible Sb_2S_3-SSCs with a narrow deviation of device efficiency.

[a]*Energy Research Division, Daegu Gyeongbuk Institute of Science & Technology, 333, Techno jungang-daero, Hyeonpung-myeon, Dalseong-gun, Daegu 711-873, Republic of Korea. E-mail: imromy@khu.ac.kr, sjsung@dgist.ac.kr; Fax: (+82) 53-785-3739; Tel: (+82) 53-785-3700*

[b]*Department of Chemical Engineering, Kyung Hee University, 1732, Deogyeong-daero, Giheung-gu, Yongin-si, Gyeonggi-do 446-701, Republic of Korea*

†Electronic supplementary information (ESI) available. See DOI: 10.1039/c4nr04148h

‡These two authors have equally contributed to this work.

To make reproducible Sb_2S_3-SSCs, the uniform thickness control of Sb_2S_3 light absorber is crucial. With this regards, the conventional CBD method has an intrinsic disadvantage because the thickness of Sb_2S_3 is significantly dependent on heterogeneous nucleation and growth processes, chemical reactions, and consequently its thickness is not linearly dependent on the reaction time. Moreover, the atomic layer deposition (ALD) is a very powerful technique to linearly control the thickness of thin films, and recently Wedemeyer *et al.*[23] demonstrated the possibility of ALD technique to form uniform Sb_2S_3 layers. Therefore, we adapted the ALD technique in order to precisely control the thickness of the Sb_2S_3 layer and to form the pure Sb_2S_3 phase. Through the systematic thickness control of the Sb_2S_3 layer, we demonstrated that highly reproducible planar Sb_2S_3-SSCs with 5.77% power conversion efficiency at 1 sun illumination could be obtained.

Experimental

The amorphous Sb_2S_3 was initially obtained by the ALD of tris-dimethylamino antimony ($Sb(N(CH_3)_2)_3$; UP Chemical Co., Ltd) and H_2S (99.5%, Matheson) gas onto a FTO/bl-TiO_2 substrate (15 Ω cm^{-1}, Pilkington) in a showerhead type ALD system (CN1 Co., Ltd, ATOMIC PREMIUM) at 130 °C. The bl-TiO_2 layer of ~70 nm thickness was deposited by spray pyrolysis and annealed at 450 °C. Pulse, exposure, and purge times of $(Sb(N(CH_3)_2)_3$ are 0.5 s, 10 s, and 10 s; Pulse and purge times of H_2S are 3 s and 10 s.

To convert the amorphous phase to crystalline one, the atomic layer deposited yellowish films of amorphous Sb_2S_3/bl-TiO_2/FTO were annealed at 330 °C for 30 min under H_2S gas. After annealing, dark-brown crystalline stibnite Sb_2S_3/bl-TiO_2/FTO was immediately removed from the heater and cool down under N_2. As an organic hole transporting material (HTM), poly-3-hexylthiophene (P3HT; Rieke metals, Inc.) was used. The solution of the HTM (15 mg mL^{-1} in 1,2-dichlorobenzene) was spin-coated onto the dense TiO_2/Sb_2S_3 layer with 2500 rpm for 60 s. Then, in order to improve the contact between P3HT and Au, a poly(3-4-ethylenedioxythiophene) doped with poly(4-styrenesulfonate) (PEDOT:PSS; Baytron AI4083) diluted with six volumes of 2-propanol was spin-coated onto the P3HT/Sb_2S_3/bl-TiO_2 at 2000 rpm for 30 s. In order to form a hybrid heterojunction, the dense TiO_2/Sb_2S_3/P3HT/PEDOT:PSS layer was annealed at 90 °C for 30 min in vacuum oven. Finally, the counter electrode was deposited by thermal evaporation of gold under a pressure of 5×10^{-6} Torr giving an active area of 0.16 cm^2 for each device.

J–V data were measured using a solar simulator (Newport, 94022A) at 1 sun condition (AM 1.5 G, 100 mW cm^{-2}) and under varied intensity of illumination by a source meter (Keithley 2400) equipped with a calibrated Si-reference cell (certified by NREL). The external quantum efficiencies (EQE) of solar cells were analyzed using an Incident Photon-to-Current Efficiency (IPCE) measurement system (McScience co., LTD, K3100) consisting of a 300 W xenon lamp, a monochromator (Spectral Products, CM110), and a multimeter (Keithley 2400). In order to eliminate experimental errors, four different cells with the same structure were fabricated using the same procedure, and all the measurements were carried out five times and averaged. Photovoltaic performance was measured by using a metal mask with an aperture area of 0.096 cm^2.

Ellipso Technology Elli-SE-aM8 variable angle spectroscopic ellipsometer was used to obtain the thickness of the Sb_2S_3 thin film and confirmed by FE-SEM (Hitachi SU8020). The UV-visible diffuse absorbance spectra of the Sb_2S_3 films were obtained using a Perkin Elmer Lambda 750 UV/VIS spectrometer with an integrating sphere. XPS spectra were obtained with an ESCALAB 250Xi (Thermo Scientific, UK) system using a microfocused (500 μm, 157 W) Al Kα X-ray beam with a photoelectron takeoff angle of 90°. A dual-beam charge neutralizer (1 eV Ar^+ and 1 eV electron beams) was used to compensate for the charge-up effect. Ar^+ ion source was operated at 3 μA and 2 kV, with rastering on an area of 4 mm × 2 mm. The XPS spectra of the CBD-Sb_2S_3 and ALD-Sb_2S_3 were obtained after Ar sputtering for 60 s. The cross-sectional morphology of the device was measured by FE-TEM (Hitachi, HF3300) with FIB systems (NB5000).

Results and discussion

Fig. 1 shows a schematic illustration of the formation of Sb_2S_3 layer on the blocking TiO_2 (bl-TiO_2)/FTO (F doped SnO_2) substrate by conventional CBD and ALD processes. In the CBD process, as illustrated in Fig. 1a, the thickness of the Sb_2S_3 layer is determined by the rate of chemical reaction, and thus the precise temperature control of the reaction bath is very important. In addition, it is very difficult to reproducibly make uniform thickness of the Sb_2S_3 layer, even in the same reaction

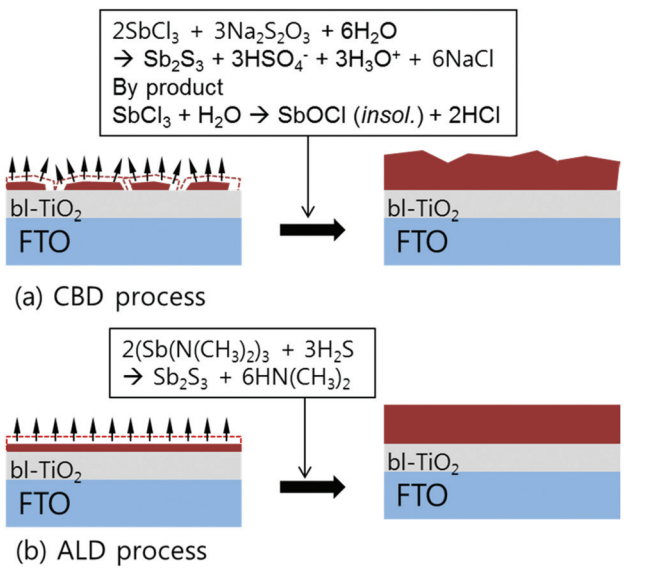

Fig. 1 Schematic illustration for the formation of Sb_2S_3 thin-layer on the bl-TiO_2/FTO substrate by CBD and ALD process.

process, because the heterogeneous nucleation condition of Sb_2S_3 on bl-TiO_2/FTO substrate will depend on the surface state of bl-TiO_2/FTO substrate. Therefore, the CBD method causes a larger thickness deviation of the Sb_2S_3 layer and makes it difficult for the Sb_2S_3-SSCs to show reproducible device performance with narrow efficiency deviation. It should also be considered that the formation of antimony oxides is inevitable when we deposit the Sb_2S_3 layer through aqueous phase chemical reaction.

On the other hand, the ALD process does not include any oxygen sources for any of the chemical reactions, and consequently it is expected that the formation of antimony oxides will be significantly suppressed. The thickness of Sb_2S_3 layer on bl-TiO_2/FTO substrate can also be precisely controlled as shown in Fig. 1b because the formation of Sb_2S_3 is physically controlled by the repeated chemical reaction of the specific amount of precursors.

Fig. 2a and b show the typical cross-sectional TEM images of the Sb_2S_3/bl-TiO_2/FTO substrates. Compared with the CBD-Sb_2S_3, the ALD-Sb_2S_3 thin layer with about 90 nm thickness was more uniformly deposited along the rough FTO/dense-TiO_2 surfaces. The magnified image of each inset shows that the ALD-Sb_2S_3 film is more densely formed than the CBD-Sb_2S_3 film because the later exhibited some pores within the film structure, which may have been formed by the thermal annealing process to convert its amorphous phase to crystalline one because the particle-like amorphous Sb_2S_3 are aggregated to form the film structure, which is converted to polycrystalline film through volume shrinkage by phase change. One of the merits of ALD process is the precise control of the thin film deposition by controlling ALD cycles. In order to investigate the deposition rate of Sb_2S_3 thin films by ALD process, we measured the thickness of Sb_2S_3 thin films with the number of ALD cycles as shown in Fig. 2c. From the thickness data quantified by spectroscopic ellipsometry, it was found that the thickness of Sb_2S_3 thin films linearly depends on the number of ALD cycles up to 4000 and the deposition rate of Sb_2S_3 was about 0.56 Å per cycle. As expected, this confirms that the ALD process can reproducibly deposit the Sb_2S_3 thin films, which will enable the Sb_2S_3-SSCs to have reproducible device efficiency. Moreover, the thickness of CBD-Sb_2S_3 films exhibited exponential increase with the deposition time and larger thickness-deviation compared to ALD-Sb_2S_3, which indicated that the device will also have larger efficiency deviation.

The purity of Sb_2S_3 sensitizer is very important because the conventional CBD-Sb_2S_3 formed in aqueous phase synthesis yields the formation of antimony oxide, and subsequently deep traps below 1.03 eV[19] from its conduction band energy are formed. The deep traps lead the injected electrons from the Sb_2S_3 sensitizer to the TiO_2 electron conductor to be transferred backward in direction and cause the recombination of electrons and holes, while deteriorating the open circuit voltage (V_{oc}). Therefore, we checked the purity of CBD-Sb_2S_3 and ALD-Sb_2S_3 using X-ray photo electron spectroscopy (XPS) spectra as shown in Fig. 3. Fig. 3a shows that the deconvolu-

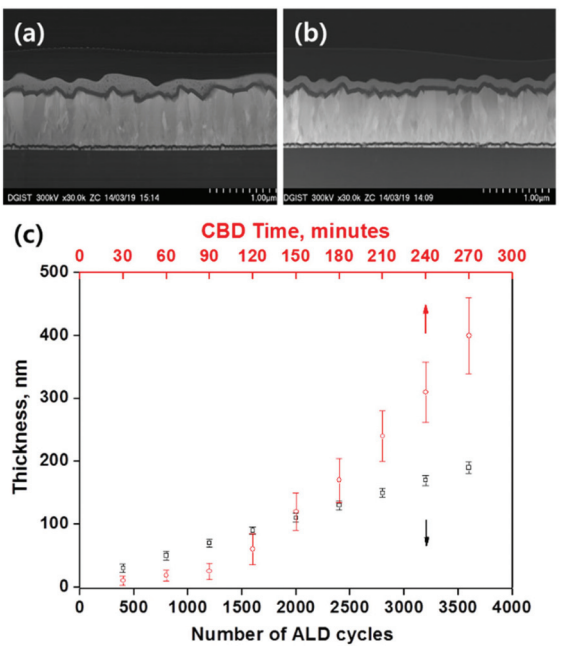

Fig. 2 A representative cross-sectional TEM image of (a) CBD-Sb_2S_3 (90 nm ± 30 nm) and (b) ALD-Sb_2S_3 (90 nm ± 6 nm) formed on bl-TiO_2 (~70 nm)/FTO (450 nm); and (c) the thickness of Sb_2S_3 layer deposited on a bare glass plate by ALD and CBD process.

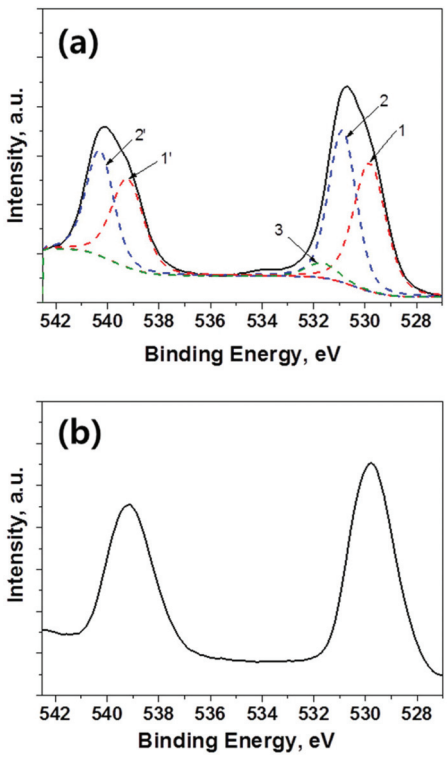

Fig. 3 XPS Sb 3d spectra of Sb_2S_3 obtained from the (a) conventional CBD process and (b) ALD process. The solid line is experimental data and dot line is fitted data. 1 (Sb_2S_3) = Sb 3d5/2, 1′ (Sb_2S_3) = Sb 3d3/2, 2 (Sb_2O_3) = Sb 3d5/2, 2′ (Sb_2O_3) = Sb 3d3/2, 3 = O 1 s.

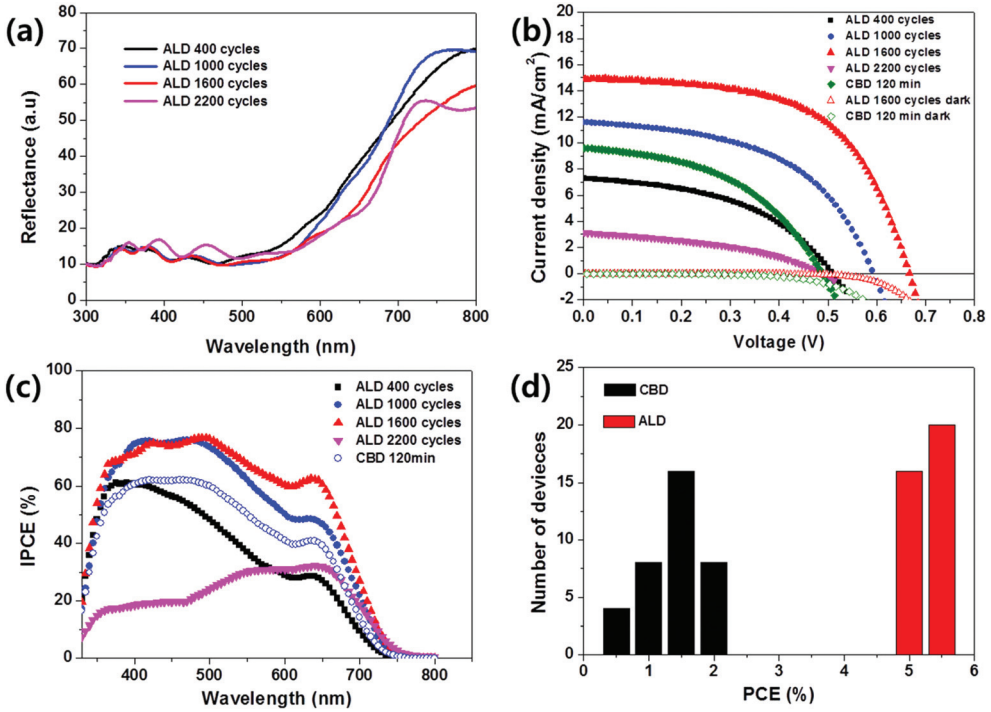

Fig. 4 (a) Diffuse reflection spectra of ALD-Sb_2S_3 deposited on bl-TiO_2/FTO substrates for various ALD cycles, (b) current density–voltage (*J*–*V*) curves, and (c) IPCE spectra of planar FTO/bl-TiO_2/Sb_2S_3/P3HT/PEDOT:PSS/Au fabricated by different ALD cycles and CBD 120 min; and (d) PCE distribution of 36 planar Sb_2S_3-SSC samples fabricated by ALD 1600 cycles and CBD 120 min.

tion of the Sb 3d core level exhibits two chemical states of Sb_2S_3 (1 and 1′), Sb_2O_3 (2 and 2′) and an overlapping oxygen peak (3). These spectra clearly confirm that the Sb_2S_3 thin films deposited by conventional aqueous CBD process contains some amount of oxide. However, XPS spectra of Sb_2S_3 deposited by ALD process showed single peaks, corresponding to a single chemical state of Sb_2S_3 (1 and 1′), and there was no oxide or oxygen peak, as shown in Fig. 3b.[22,24] From these XPS analyses, it was found that high quality Sb_2S_3 thin films without any oxide or oxygen impurities could be successfully deposited by ALD process, which might be advantageous for achieving high performance Sb_2S_3 solar cells.

Fig. 4a shows the diffuse reflection spectra of ALD-Sb_2S_3 with the number of repeated ALD cycles, where the thickness of ALD 400, 1000, 1600, and 2200 cycles correspond to 30 nm ± 6 nm, 60 nm ± 7 nm, 90 nm ± 6 nm, and 120 nm ± 7 nm. The absorption tail is gradually red-shifted with the thickness of ALD-Sb_2S_3 layer and is almost saturated over ALD 1600 cycles. Fig. 4b and Table 1 show the current density–voltage (*J*–*V*) curves and the photovoltaic parameters (short circuit current density, open circuit voltage, fill factor, and power conversion efficiency: J_{sc}, V_{oc}, FF, and η) of CBD- and ALD-Sb_2S_3 devices. A conventional FTO/bl-TiO_2/CBD-Sb_2S_3/P3HT/Au device showed V_{oc} of 0.4886 V, J_{sc} of 9.63 mA cm^{-2}, FF of 46.13%, and η of 2.17%, which are similar in result with previously reported planar Sb_2S_3-SSCs (V_{oc} = 0.56 V, J_{sc} = 7.15 mA cm^{-2}, FF = 35%, η = 1.43%).[25] Here, it is noted that the CBD 120 min sample exhibited the best device efficiency when we checked the efficiency of planar Sb_2S_3-SSCs with the CBD time (the thickness of CBD-Sb_2S_3 120 min sample is shown in Fig. 2a).

Table 1 Summary of device performance for planar Sb_2S_3-SSCs. Metal mask (0.096 cm^2) was attached to each cell before measurement under illumination (100 mW cm^{-2})

Sb_2S_3 (cycles)	V_{oc} (V)	J_{sc} (mA cm^{-2})	FF (%)	η (%)
ALD 400	0.5105	7.28	46.17	1.72
ALD 1000	0.5937	11.60	51.15	3.52
ALD 1600	0.6665	14.92	58.04	5.77
ALD 2200	0.4872	3.13	40.54	0.62
CBD 120 min	0.4886	9.63	46.13	2.17

On the other hand, FTO/bl-TiO_2/ALD-Sb_2S_3/P3HT/Au devices exhibited dramatically enhanced photovoltaic performance, depending on the ALD cycles of Sb_2S_3; the J_{sc} enhanced with increased ALD cycle of Sb_2S_3 up to 1600 cycles, and then decreased with further increase in the ALD cycle. We also confirmed the enhancement of V_{oc} with an increase of the ALD cycle of Sb_2S_3 up to 1600 cycles, and then a decrease of V_{oc} with the 2200 ALD cycle. All of ALD-Sb_2S_3 solar cells showed higher V_{oc} value compared with CBD-Sb_2S_3, which might be attributed to the formation of more pure Sb_2S_3 absorbers without impurities as confirmed by XPS analysis in Fig. 3. The best device under air mass 1.5 global (AM 1.5 G) and full sunlight (100 mW cm^{-2}) exhibited J_{sc}, V_{oc}, and FF values of 14.92 mA cm^{-2}, 0.667 V, and 58.04%, respectively, yielding η of

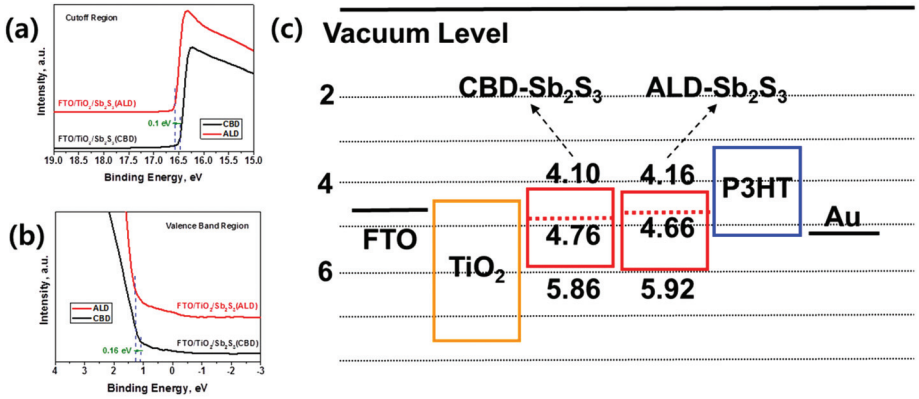

Fig. 5 UPS spectra at (a) cutoff region, and (b) valence band region for FTO/bl-TiO_2/ALD-Sb_2S_3 and FTO/bl-TiO_2/CBD-Sb_2S_3 samples; and (c) corresponding energy band diagram of planar ALD-Sb_2S_3- and CBD-Sb_2S_3-SSC.

5.77%, which is three-fold higher than that of the CBD Sb_2S_3 device.

In order to investigate the light response of Sb_2S_3 devices, we measured IPCE (Incident photon-to-current conversion efficiency) of CBD-Sb_2S_3 and ALD-Sb_2S_3 thin film solar cells (Fig. 4c). Compared with CBD-Sb_2S_3, ALD-Sb_2S_3 solar cells with 1000 and 1600 ALD cycle showed higher IPCE, although the absorption spectra edges of CBD-Sb_2S_3 and ALD-Sb_2S_3 were the same near 750 nm wavelength because the average thickness of Sb_2S_3 (CBD 120 min and ALD 1000 cycles) was the same to ~90 nm (see Fig. 2a and b).

It should be noted that despite planar type solar cells, the planar ALD-Sb_2S_3-SSCs exhibited excellent photovoltaic performance compared with the planar CBD-Sb_2S_3 device and the mesoscopic CBD-Sb_2S_3-SSCs with P3HT hole conductor.[26] The improved performance of ALD-Sb_2S_3 solar cells might be attributed to the high purity Sb_2S_3 absorbers compared with conventional CBD-Sb_2S_3 absorbers because (1) the dark current leakage of ALD-Sb_2S_3 sample could be blocked even at higher bias voltage than that of the CBD-Sb_2S_3 sample as shown in Fig. 4b, which consequently enables the ALD-Sb_2S_3 to have higher V_{oc};[27] and (2) the charge transfer and/or the charge collection efficiency of the ALD-Sb_2S_3 sample could be significantly improved from those of the CBD-Sb_2S_3 sample, owing to the similar light harvesting efficiency at same thickness of Sb_2S_3 absorber, since IPCE is the product of light harvesting efficiency, charge transfer efficiency, and charge collection efficiency.

From thickness analysis of ALD-Sb_2S_3 thin films (Fig. 2), it was found that the controllability and uniformity of ALD-Sb_2S_3 films were considerably better than those of the conventional CBD-Sb_2S_3. This reproducible formation of Sb_2S_3 with small thickness-deviations by ALD process will guarantee the reproducibility of solar cell devices with small efficiency-deviations, which is a crucial factor for commercialization of solar cells. To confirm the reproducibility of solar cell devices, the PCE (η) histogram of each individually fabricated solar cell device using CBD-Sb_2S_3 and ALD-Sb_2S_3 was exhibited, as shown in Fig. 4d. The PCE histogram indicates that ALD-Sb_2S_3 solar cells show not only higher PCE, but also narrow distribution of PCE compared with CBD-Sb_2S_3 solar cells. This result shows that the ALD process for the formation of Sb_2S_3 absorbers is a promising fabrication tool for reproducible solar cells.

Fig. 5a and b show the UPS spectra of Sb_2S_3 films deposited on bl-TiO_2 by CBD and ALD processes. The work function is determined from the photon energy and the high binding energy cutoff of the UPS spectrum, corrected for a −5 V bias. The high binding energy cutoff is 16.56 and 16.46 V for ALD-Sb_2S_3 and CBD-Sb_2S_3, respectively (Fig. 5a), and low binding energy onset of ALD-Sb_2S_3 and CBD-Sb_2S_3 is 1.26 and 1.10 V, respectively (Fig. 5b). The work function was calculated by the equation, Φ = 21.22 – high binding energy cutoff, giving the position of the Fermi level as 4.66 and 4.76 eV for ALD-Sb_2S_3 and CBD-Sb_2S_3, respectively. By adding the low binding energy onset to the UPS spectrum, the valence band maximum with respect to the vacuum level can be calculated. The conduction band minimum is determined by adding an optical band gap of Sb_2S_3, 1.76 eV, which is estimated from the IPCE spectra (Fig. 4c). From these results, it was possible to illustrate the energy band diagrams of the ALD-Sb_2S_3 and CBD-Sb_2S_3 devices (Fig. 5c). The ALD-Sb_2S_3 showed 0.1 eV higher Fermi levels compared with the CBD-Sb_2S_3, which might be attributed to the formation of purer Sb_2S_3 sensitizers by the ALD process, because the oxide impurities make defect states in Sb_2S_3 absorbers and consequently the V_{oc} is deteriorated. Therefore, the higher V_{oc} of ALD-Sb_2S_3-SSCs compared with that of CBD-Sb_2S_3-SSCs, as shown in Fig. 4 and Table 1, could be explained by the higher Fermi-level of ALD-Sb_2S_3 absorbers.

Conclusions

We could fabricate reproducible planar Sb_2S_3-SSCs with 5.77% power conversion efficiency with narrow efficiency-deviation by ALD technique, whereas the planar Sb_2S_3-SSCs fabricated by the conventional CBD method exhibited poor power conversion efficiency with wide deviation. The high reproducibility of

ALD-Sb_2S_3-SSCs was attributed to the conformal deposition of very uniform Sb_2S_3 thin-layers with narrow deviation on bl-TiO_2/FTO substrate. Moreover, the CBD method yielded the formation of rough Sb_2S_3 thin-layers with wide deviation because the deposition rate of Sb_2S_3 thin-layers was nonlinear to reaction time and very sensitive to reaction temperature. The high device efficiency was attributed to the formation of pure Sb_2S_3 free of oxide because no oxygen source is involved during the entire ALD process, whereas the aqueous phase based CBD inevitably forms antimony oxide. Therefore, the ALD-Sb_2S_3-SSCs exhibited high open circuit voltage, short circuit current density, and high fill factor due to the reduced backward recombination by large suppression of oxide defects within the Sb_2S_3-sensitizers.

Acknowledgements

This work was supported by DGIST R&D Program of the Ministry of Education, Science and Technology of Korea (14-EN-03).

Notes and references

1 B. O'regan and M. Grätzel, *Nature*, 1991, **353**, 737.
2 S. Mathew, A. Yella, P. Gao, R. Humphry-Baker, B. F. Curchod, N. Ashari-Astani, I. Tavernelli, U. Rothlisberger, M. K. Nazeeruddin and M. Grätzel, *Nat. Chem.*, 2014, **6**, 242.
3 A. J. Nozik, *Chem. Phys. Lett.*, 2008, **457**, 3.
4 R. Costi, A. E. Saunders and U. Banin, *Angew. Chem., Int. Ed.*, 2010, **49**, 4878.
5 Y. L. Lee and Y. S. Lo, *Adv. Funct. Mater.*, 2009, **19**, 604.
6 J. H. Bang and P. V. Kamat, *Adv. Funct. Mater.*, 2010, **20**, 1970.
7 S. H. Im, Y. H. Lee and S. I. Seok, *Electrochim. Acta*, 2010, **55**, 5665.
8 S. H. Im, Y. H. Lee, S. I. Seok, S. W. Kim and S.-W. Kim, *Langmuir*, 2010, **26**, 18576.
9 S. H. Im, H.-j. Kim, S. W. Kim, S.-W. Kim and S. I. Seok, *Energy Environ. Sci.*, 2011, **4**, 4181.
10 J. Jean, S. Chang, P. R. Brown, J. J. Cheng, P. H. Rekemeyer, M. G. Bawendi, S. Gradečak and V. Bulović, *Adv. Mater.*, 2013, **25**, 2790.
11 J. Y. Kim, O. Voznyy, D. Zhitomirsky and E. H. Sargent, *Adv. Mater.*, 2013, **25**, 4986.
12 Y. Itzhaik, O. Niitsoo, M. Page and G. Hodes, *J. Phys. Chem. C*, 2009, **113**, 4254.
13 S.-J. Moon, Y. Itzhaik, J.-H. Yum, S. M. Zakeeruddin, G. Hodes and M. Grätzel, *J. Phys. Chem. Lett.*, 2010, **1**, 1524.
14 S. H. Im, H.-j. Kim, J. H. Rhee, C.-S. Lim and S. I. Seok, *Energy Environ. Sci.*, 2011, **4**, 2799.
15 S. H. Im, C.-S. Lim, J. A. Chang, Y. H. Lee, N. Maiti, H.-J. Kim, M. K. Nazeeruddin, M. Grätzel and S. I. Seok, *Nano Lett.*, 2011, **11**, 4789.
16 Y. C. Choi, Y. H. Lee, S. H. Im, J. H. Noh, T. N. Mandal, W. S. Yang and S. I. Seok, *Adv. Energy Mater.*, 2014, **4**, 1301680.
17 K. Tsujimoto, D.-C. Nguyen, S. Ito, H. Nishino, H. Matsuyoshi, A. Konno, G. R. A. Kumara and K. Tennakone, *J. Phys. Chem. C*, 2012, **116**(25), 13465.
18 S. Ito, K. Tsujimoto, D.-C. Nguyen, K. Manabe and H. Nishino, *Int. J. Hydrogen Energy*, 2013, **38**, 16749.
19 Y. C. Choi, D. U. Lee, J. H. Noh, E. K. Kim and S. I. Seok, *Adv. Funct. Mater.*, 2014, **24**, 3587.
20 S. Messina, M. Nair and P. Nair, *Thin Solid Films*, 2007, **515**, 5777.
21 D. U. Lee, S. W. Pak, S. G. Cho, E. K. Kim and S. I. Seok, *Appl. Phys. Lett.*, 2013, **103**, 023901.
22 N. Maiti, S. H. Im, C.-S. Lim and S. I. Seok, *Dalton Trans.*, 2012, **41**, 11569.
23 H. Wedemeyer, J. Michels, R. Chmielowski, S. Bourdais, T. Muto, M. Sugiura, G. Dennler and J. Bachmann, *Energy Environ. Sci.*, 2013, **6**, 67.
24 C. P. Liu, H. E. Wang, T. W. Ng, Z. H. Chen, W. F. Zhang, C. Yan, Y. B. Tang, I. Bello, L. Martinu, W. J. Zhang and S. K. Jha, *Phys. Status Solidi B*, 2011, **249**, 627.
25 P. P. Boix, Y. H. Lee, F. Fabregat-Santiago, S. H. Im, I. Mora-Sero, J. Bisquert and S. I. Seok, *ACS Nano*, 2011, **6**, 873.
26 J. A. Chang, S. H. Im, Y. H. Lee, H.-j. Kim, C.-S. Lim, J. H. Heo and S. I. Seok, *Nano Lett.*, 2012, **12**, 1863.
27 J. Y. Hwang, S. A. Lee, Y. H. Lee and S. I. Seok, *ACS Appl. Mater. Interfaces*, 2010, **2**, 1343.